Medizinische Fakultät

der

Universität Duisburg-Essen

Translational Skin Cancer Research (TSCR)

DKTK Partner Site Essen/ Düsseldorf German Cancer Research Center (DKFZ)

University Duisburg Essen

The HDAC inhibitor domatinostat promotes cell cycle arrest, induces apoptosis and increases immunogenicity of virus-positive Merkel Cell Carcinoma cells

Inaugural – Dissertation
zur
Erlangung des Doktorgrades der Medizin

durch die Medizinische Fakultät

der Universität Duisburg-Essen

Vorgelegt von

Lina Song

Aus Anhui in China

2020

DuEPublico
Duisburg-Essen Publications online

UNIVERSITÄT DUISBURG ESSEN
Offen im Denken

ub universitäts bibliothek

Diese Dissertation wird über DuEPublico, dem Dokumenten- und Publikationsserver der Universität Duisburg-Essen, zur Verfügung gestellt und liegt auch als Print-Version vor.

DOI: 10.17185/duepublico/72836
URN: urn:nbn:de:hbz:464-20201006-110757-6

Dieses Werk kann unter einer Creative Commons Namensnennung 4.0 Lizenz (CC BY 4.0) genutzt werden.

Dean: Herr Univ.-Prof. Dr. med. J. Buer

1.Gutachter: Herr Univ.-Prof. Dr. med. J. C. Becker

2. Gutachter: Herr Univ.-Prof. Dr. med. B. Scheffler

Tag der mündlichen Prüfung: 18. September 2020

- **Publications:**

1. *Youzhou Sang#, Yanxin Li#,* ***Lina Song#,*** *Angel A. Alvarez#, Weiwei Zhang, Deguan Lv, Jianming Tang, Feng Liu, Zhijie Chang, Shigetsugu Hatakeyama, Bo Hu, Shi-Yuan Cheng, Haizhong Feng,* TRIM59 promotes gliomagenesis by inhibiting TC45 dephosphorylation of STAT3. Cancer Res. 2018; 78:1792–1804. doi: 10.1158/0008-5472.CAN-17-2774.
2. ***Lina Song****, Haizhong Feng. Promotion of* Trim59 on neuroglioma genesis. J SJTU. 2017; Vol. 37, doi: 10.3969/j.issn.1674-8115.2017.06.002
3. *Deguan Lv#, Yanxin Li#, Weiwei Zhang, Angel A. Alvarez,* ***Lina Song****, Jianming Tang, Wei-Qiang Gao, Shi-Yuan Cheng, Haizhong Feng,* TRIM24 is an oncogenic transcriptional co-activator of STAT3 in glioblastoma. Nat Commun. 2017; 8: 1454. doi: 10.1038/s41467-017-01731-w
4. *Lei Zhang#, Weiwei Zhang#, Yanxin Li#, Zuo-qing Li, Yin-fang Wang,* ***Lina Song****, Deguan Lv, Ichiro Nakano, Bo Hu, Shi-yuan Cheng, Haizhong Feng,* SHP-2-upregulated ZEB1 is important for PDGFRα-driven glioma epithelial–mesenchymal transition and invasion in mice and humans. Oncogene. 2016 Oct 27; 35(43): 5641–5652. doi: 10.1038/onc.2016.100

- **Conference paper:**

1. ***Lina Song****, AnneCatherine Bretz, Jan Gravemeyer, Ivelina Spassova, SvetlanaHamm, Shakhlo Muminova, Rene Bartz and Juergen C. Becker,* Abstract 2368: Domatinostat increases apoptosis, G2M cell-cycle arrest and immunogenicity of Merkel cell carcinoma. Cancer Res. 2019; doi: 10.1158/1538-7445. AM2019-2368

Table of Contents

1. Introduction

1.1 Merkel cell carcinoma

Merkel cell carcinoma (MCC) is a rare but highly aggressive cutaneous neuroendocrine cancer, occurring preferentially in elderly or immune-compromised patients. MCC typically manifests as a rapidly developing, painless tumor on sun-exposed areas of the skin (North *et al*., 2019). First histopathological characterizations of this tumor include the trabecular carcinoma of the skin (Toker, 1972) with an unknown cell of origin. The name was changed to 'Merkel cell carcinoma' once phenotypic similarities were observed between the tumor cells and Merkel cells. Merkel cells, found in the basal layer of the epidermis around hair follicles, and function as mechanoreceptors stimulated by of touch – and are thus relevant to afferent sensory nerves – but also display neuroendocrine features (Becker *et al*., 2017).

MCC development is induced mainly by chronic exposure to ultraviolet light (UV) or clonal integration of the Merkel cell polyomavirus (MCPyV), also known as human polyomavirus (Becker *et al*., 2017). The connection of MCC incidence and solar UV radiation was already verified during 1986-1999 in the USA (Miller and Rabkin, 1999). In addition, since individuals with darker skin show a distinctly lower risk of MCC compared to populations with light skin, pigmentation of the skin is discussed as a vital protection against MCC development (Stang *et al*., 2018). MCPyV, a small non-enveloped double stranded DNA virus, like other polyoma viruses encodes early transforming genes, i.e., the large and small T antigens. Both antigens have been shown to regulate cell cycle relevant genes as well as tumor suppressor genes in MCPyV-positive MCC cell lines (Li *et al*., 2013). Furthermore, large T antigen plays an essential role in MCC cell proliferation via inactivation of retinoblastoma protein (Rb), a tumor suppressor protein (Hesbacher *et al*., 2016).

Important risk factors for MCC development include immunosuppression and old age. Immunosuppressed solid organ transplant recipients or AIDS patients are more susceptible to

develop MCC compared to immunocompetent patients (Ma and Brewer, 2014). Due to increasing life expectancy and rising numbers of immunocompromised patients, the steady ascent of MCC incidence is not surprising. Treatment of MCC consists of wide-local excision, followed by adjuvant radiotherapy. Until recently, prognosis for patients with advanced MCC not amendable by these therapy options was considered infaust.

This dramatically changed with the introduction of immunotherapy by immune checkpoint inhibitors, *i.e.*, monoclonal antibodies interfering with programmed cell death protein 1 (PD-1) or its ligand (PD-L1), both demonstrating remarkable therapy response rates (Kaufman *et al*., 2018, Nghiem *et al*., 2019). Unfortunately, about half of the patients either show primary or develop secondary resistances to these immune checkpoint inhibitors (Spassova *et al*., 2020) via immune escape mechanisms, which may be mediated amongst others via reduction or loss of major histocompatibility complex (MHC) class I surface expression (Paulson *et al*., 2014, Paulson *et al*., 2018, Ritter *et al*., 2017). Loss of MHC class I surface expression can be caused by impairment of HLA gene expression (Raffaghello *et al*., 2005), lack of β_2-microglobulin (β2m) expression (Sade-Feldman *et al*., 2017), or MHC class I molecule instability due to lack of peptide binding to the HLA class I groove (Ritter *et al*., 2017). The latter originated from a defective expression and/or function of the antigen processing and presentation machinery (APM) (Cai *et al*., 2018).

1.2 HDAC and HDAC inhibitor

Histone deacetylases (HDACs) are a specific class of enzymes that catalyze deacetylation of proteins, particularly histones. HDACs are categorized in four classes depending on their sequence homology to yeast enzymes and their domain organization. Class I HDACs are primarily present in the nucleus, whereas the other classes are found both in the nucleus and the cytoplasm (Kong *et al*., 2011). Aberrant expression and regulation of HDACs often occur

in cancer, suggesting a critical role of these enzymes in tumorigenesis (Li and Seto, 2016). Similarly, disparate acetylation of non-histone proteins involved in cell cycle and apoptosis regulation is normalized upon HDAC inhibition (Li *et al*., 2016). Furthermore, several lines of evidence suggest an immunogenic impact of HDAC inhibition (Conte *et al*., 2018) such as induction of cancer germline antigens (Moreno-Bost *et al*., 2011), T cell recruiting chemokines (Zheng *et al*., 2016) and APM component genes TAP1, TAP2, LMP2 and LMP7 (Setiadi *et al*., 2008). Indeed, my lab has previously reported, that in MCC cell lines as well as in tumor tissues, reduced APM component gene expression can be normalized by treatment with broad-spectrum HDAC inhibitors such as vorinostat or panobinostat (Ritter *et al*., 2017, Ugurel *et al*., 2019). The clinical use of broad spectrum HDAC inhibitors is well established (West *et al*., 2014). However, HDAC class I inhibitors are currently regarded as even more promising agents for the treatment of cancer, mainly due to a strong induction of cell cycle arrest (Ververis *et al*., 2013).

Hence, we scrutinized the effects of domatinostat (aka 4SC-202), an orally available small molecule inhibitor selectively targeting class I HDACs (HDAC 1, 2 and 3), since it is currently be tested be clinically tested in the treatment of patients with advanced MCC in combination with the anti-PD-L1 antibody avelumab[1]. Domatinostat also inhibits the lysine-specific histone demethylase 1A (LSD1) at low μM concentrations (von Tresckow *et al*., 2019). A notion, which may additionally explain some of the differences of its activity compared to other HDAC inhibitors, its true work mechanism is yet not fully established (Haydn *et al*., 2017). To add some additional information on domatinostat's impact on neoplastic cells, we report here that it causes G2M arrest and apoptosis in a fraction of MCC cells; in the remaining viable cells, it

[1] Bartz R, Behling T, Reimann P, Hermann F. Preclinical rationale and clinical design for the combination of domatinostat with avelumab in Merkel Cell Carcinoma patients: the MERKLIN and MERKLIN 2 studies. 1st International Symposium on Merkel Cell Carcinoma; 21. – 22. Oct. 2019, Tampa, Florida, USA

strongly induces APM component gene transcription resulting in increased HLA class I surface expression.

2. Materials and Methods

2.1 MCC cell lines and cell culture

The MCPyV-positive MCC cell lines WaGa, MKL-1 and MKL-2 have been described before (Houben *et al*., 2010). The MCPyV-positive MCC suspension cell line WaGa was established from the MCC of a 67-year old male patient from the Dermatology Department at the University Hospital Würzburg (Germany) and from the Department of Translational Dermato-Oncology (DKTK) in the University Hospital Essen (Essen, Germany). As stated by Paulson *et al*., the MCPyV-positive MCC suspension cell line MKL-1 was established from a 26-year-old male patient with nodal metastasis in the University of Pittsburgh Cancer Institute, University of Pittsburgh (United States of America) by Masahiro Shuda. MKL-2, also known as the MCPyV-positive MCC suspension cell line, was derived from a Caucasian 72-year-old male in the Northwestern University at the Robert H. Lurie Comprehensive Cancer Center (Chicago, IIIinois, United States of America). All cell lines were cultured under standard conditions (37 °C; 5% CO_2) in RPMI-1640 medium (PAN Biotech, Aidenbach, Germany) supplemented with 10% fetal bovine serum (FBS; PAN Biotech) and 1% penicillin-streptomycin (P/S; PAN Biotech). Primary skin fibroblasts isolated from healthy skin were cultured in DMEM and DMEM/F12 (1:1) medium (Lonza, Cologne, Germany) supplemented with 10% FBS and 1% P/S. Cell lines were regularly tested to ensure absence of mycoplasma and identification via DNA fingerprinting (last performed in June 2019). Before trypsinization, all cells were washed with PBS (with or without magnesium and calcium); the process was performed with pre-warmed trypsin and EDTA (T/E, containing 0.05% trypsin and 0.02% EDTA) in a 37°C water bath. Cells were cryopreserved in sterile cryo tubes in 10% DMSO and

FBS; slow freezing procedure was ensured by controlled rate freezing apparatus. Authentication of the cells used were performed prior to the experiments.

For treatment with the HDAC inhibitor domatinostat (4SC AG, Planegg-Martinsried, Germany) or nocodazole (Sigma-Aldrich, Darmstadt, Germany), cells were seeded in 6-well or 12-well plates at a concentration of $1x10^6$ cells/ml. Domatinostat was dissolved in DMSO (PanReac AppliChem, Darmstadt, Germany). Domatinostat and nocodazole were used at the indicated concentrations. Primary skin fibroblasts (16-6938-BO) were acquired from the University Clinic Essen and grown from healthy skin tissue. To quantify the number of viable cells, trypan blue exclusion assay was used. Dead cells were removed by Ficoll-Paque (Biochrom, Berlin, Germany) density centrifugation. Since MKL-1 and MKL-2 cells are spheroid growing cell lines, to obtain single cells, a particular protocol is needed: collect cell suspension and centrifuge cells at 300 rcv (G) for 5 minutes, then discard supernatant and resuspend cell pellet in 2 ml trypsin EDTA (T/E) by pipetting up and down 5 to 10 times, afterwards, stir the tube in water bath at 37°C for 5 minutes, add 2 ml cell culture medium to stop the T/E reaction and centrifuge the mixture at 1500 rpm for 5 minutes, discard supernatant and resuspend cell pellet in 1ml PBS up and down for 5-10 times, to detect the effect, add 1ml 7-AAD to cell suspension and use 40 µm cell strainer to get the final singlets, FACS can be used to detect the effect of obtain singlets.

2.2 Analysis of cell viability

To distinguish between viable and dead cells within a cell suspension, trypan blue exclusion test was used. Under the microscope, viable cells with intact cell membranes appear with a clear cytoplasm while nonviable or dead cells stained with trypan blue, will be presented with a blue cytoplasm (Strober, 2015). To quantify the number of viable cells, cell suspensions were mixed and incubated at a ratio of 1:1 with trypan blue. Cell viability was calculated by dividing the

number of viable cells by the number of all cells within the 4 grids on the hemocytometer. The protocol to define the cell density of cells suspended on a hemocytometer includes:

1. Prepare solution of trypan blue dye with concentration of 0.4% diluted in buffered isotonic salt solution (PH 7.2 to 7.3)
2. Add 20µl of cell suspension to 20µl stock solution of trypan blue
3. Load the hemocytometer with mixture of cell suspension and trypan blue and check under the microscope immediately at a low magnification
4. Count the viable cells with intact membrane and number of total cells.
5. To determine the viability, present as follows: % viable cells = (Number of viable cells /Number of total cells) ×100.
6. Correct the viability for the dilution factor (Number of viable cells $\times 10^4 \times 2$ (dilution folds).

2.3 Enrichment of viable cells

In order to eliminate dead cells and enrich for viable cells, cell suspensions were diluted 1:1 with 1x PBS and carefully layered on top of an equal volume of biocoll solution (Biochrom, L6115). Cell suspensions were separated by centrifugation (20 min at 1200 g, low acceleration, no brakes). The layer with viable cells on the interface between PBS and biocoll was transferred to a fresh tube. After washing with PBS, cells were pelleted by centrifugation and resuspended in PBS or cell culture medium. Number of viable cells were determined and cells were further processed according to specific experimental requirements.

2.4 scRNA-seq and gene expression analysis

Since WaGa cells grows in suspension, no isolation step was required and MCC cells were directly single-cell barcoded using the 10x Genomics 3' Chromium v2.0 platform (Zheng *et al*., 2017). Library preparation was performed according to the 10x Genomics protocol

instruction (https://support.10xgenomics.com/single-cell-gene-expression/library-prep). Afterwards, the libraries were sequenced on an Illumina HiSeq 4000. The Cell Ranger Single Cell Software Suite version 2.1.1 (http://10xgenomics.com/) was used with default settings to separately align cDNA reads to the hg19 human reference genome and the Merkel cell polyomavirus sequence (NC_010277.2). For quality control, cells with less than 1000 UMI counts, no more than 200 genes or expression exceed 10% mitochondrial genes were removed leaving in total 4187 cells. The Seurat R package was downloaded and used for normalization as well as biological analysis (Butler *et al*., 2018). Expression data in the count matrix was then imputed after the process of normalization with the software package MAGIC (Newton *et al*., 2017). Afterwards, the data was aggregated into one single file and imported into the Loupe browser v2.0.0 (http://10×genomics.com/) and R. Single-cell gene expression was visualized by U-MAP for dimension reduction. For cell cycle annotation, signatures were calculated using marker genes reported by Kowalczyk et al (Kowalczyk *et al*., 2015). Pathway analysis of significantly regulated genes (adjusted P-value < 0.1) was performed with Metascape (http://metascape.org) on line using default settings. Metascape is a free used gene annotation and analysis tool offering automated meta-analysis methods to annotate expressed genes to common or unique pathways as well as constructing protein networks among orthogonal targeted discovery studies.

For gene set enrichment analysis (GSEA), GSEA version 3.0 was used (Subramanian *et al*, 2005). A priori gene sets were used for Gene set enrichment analysis; the gene sets were grouped according to their involvement in the same biological signal cascade, or through proximal site on a chromosome. A database for these predefined gene sets can be observed at the *Molecular signatures database* (MSigDB). GSEA, DNA microarrays and RNA-seq are still used and compared between two categories, rather than bringing the individual genes with a long list into focus, the point is put on a gene set. Researchers scrutinize if most genes in the gene set take up with the extremes of the list: the top and bottom stand for the big differences

in expression between the two cell types. In case the gene set groups at the top (over-expressed) or bottom (under-expressed), it is considered to be associated with phenotypic differences.

2.5 Cell cycle analysis

To examine the effect of domatinostat on cellular proliferation and cell cycle, the incorporation rate of Bromodesoxyuridine (BrdU) was measured. Seed cells (2 million per well) to 6-well plates at the final concentration at 10^6 per well. Cells were pulse-labeled with BrdU (2.5 µg/mL, BioLegend, Koblenz, Germany): add 4 µl BrdU stock solution to each well. After 2 hours of incubation cells (500 µl cell suspension) were transferred to centrifuge tube and trypsin (500 µl TE, 5 minutes incubation in 37°C water bath) was added to spheroid cells to receive single cells. Samples were centrifuged, cell pellet was washed with 1 ml magnetic-activated cell sorting (MACS) buffer, vortexed and centrifuged again. Subsequently, cells were washed with PBS and fixed with 70 % ethanol for 30 minutes on ice. After denaturation with 1.5 M HCl for 30 minutes at room temperature (RT), cells were washed with PBS (PAN Biotech) and resuspended in 100-300 µl of MACS buffer with 2.5 µl FITC-labeled anti-BrdU monoclonal antibody (clone 3D4, Biolegend). After Incubating for 30 minutes at RT, wash cells with PBS and resuspend in 300 µl MACS. Prior to flow cytometric analysis, 1 µl of 7-aminoactinomycin (7-AAD; 10 µg/ml, Abcam, Berlin, Germany) was added to each sample to determine the absolute DNA quantity of cells. Ten thousand events were analyzed on a flow cytometer (Cytoflex, Beckman Coulter Life Science, Krefeld, Germany) and gates were adjusted to quantify cell cycle populations (G0/G1, S, G2M). Data was analyzed using FlowJo TM V10.6.1 (Becton Dickinson (BD), Franklin Lakes, USA).

2.6 Apoptosis assays

Before treatment, viable MCC cells were enriched by biocoll gradient and then seeded. Seed cells (1×10^6 cells) in two 6-well plates (in triplicates). One served as domatinostat treatment group, the other as control group without any treatment. To determine cellular apoptosis, the NucView 488/MitoView 633 Apoptosis Assay Kit (Biotium, Fremont, United States) was used according to the manufacturer's instructions. The kit contains Caspase-3 Substrate (NucView®488) and mitochondrial dye (MitoView^{TM}633). The kit provides a convenient method to detect apoptotic cells according to caspase-3 activity and variation of cell mitochondrial membrane potential by flow cytometry as well as fluorescence microscopy. Importantly, NucView®488 Caspase-3 Substrate is designed to detect both intracellular caspase-3 and stain the cell nucleus which undergoes morphological changes during apoptosis. MitoView^{TM}633 mitochondrial dye is a far-red fluorescent mitochondrial dye that is detected based on the mitochondrial membrane potential. Apoptotic cells with intact membrane potential exhibit a much weaker red MitoView^{TM}633 mitochondrial dye staining than healthy cells. Primary fibroblasts treated for 24h with 200 nM H_2O_2 were used as a positive control. The detailed assay protocol including the follow several steps: warming up staining medium with MitoView^{TM}633 and NucView®488 in advance, for example, add 1 µl MitoView^{TM}633 and 1 µl NucView®488 to 200 µl cell culture medium and mix well; pellet the cells, discard supernatant and resuspend with fresh staining medium; incubate cells at 37°C for 15 minutes or days; analyze fluorescence under fluorescence microscope (apoptotic cells stained blue while healthy cells stained red with intact mitochondrial potential) and flow cytometry. Viable and apoptotic cells were visualized by fluorescence microscopy (Zeiss Axio Observer.Z1, Oberkochen, Germany) and quantified by flow cytometry. Data was analyzed using the CytExpert version 2.3 software (Beckman Coulter, Krefeld, Germany). For higher resolution, coverslips were coated before adding apoptosis dyes, the detailed protocol is: prepare 100ul Poly-L-lysine on Para film; place coverslip face down in a 12 well plate; wash with 1ml PBS;

add 1ml of cell suspension; put the 12 well plate in cell culture incubator for 30 minutes; discard cell supernatant and wash cells with PBS; add apoptosis dyes and put the plate back to cell culture incubator ranging from 10 min to days (the samples can be measured after 10 minutes).

2.7 Quantitative real time polymerase chain reaction (qRT-PCR)

PeqGOLD total RNA kit was used to isolate RNA (VWR/Peqlab, Erlangen, Germany) followed by transcription into cDNA using the SuperScript IV reverse transcriptase (ThermoFisher, Dreieich, Germany) according to the manufacturer's instructions. qRT-PCR was performed on the CFX Real-Time PCR system (Bio-Rad Laboratories, Düsseldorf, Germany). RPLP0 (housekeeping gene) served as an endogenous control and was detected with specific primers and a TaqMan probe: 6-FAM-YY-ATCTGCTGCATCTGCTTGGAGCCCA-BHQ1 (Applied Biosystems, Darmstadt, Germany). The mRNA expression of TAP1, TAP2, LMP2 and LMP7 was detected using SYBR green assays (Sigma-Aldrich, Darmstadt, Germany) with primers listed in Supplementary Table 1. Relative quantification was calculated by the ΔΔCt method.

Primer list: Table1

	forward	**reverse**
HLA-A	GCGGCTACTACAACCAGAGC	GATGTAATCCTTGCCGTCGT
B2M	TCTCTGCTGGATGACGTGAG	TAGCTGTGCTCGCGCTACT
TAP1	TCAGGGCTTTCGTACAGGAG	TCCGGAAACCGTGTGTACTT
TAP2	ACTGCATCCTGGATCTCCC	TCGACTCACCCTCCTTTCTC
LMP2 (PSMB9)	TCAAACACTCGGTTCACCAC	GGAGAAGTCCACACCGGG
LMP7 (PSMB8)	CATGGGCCATCTCAATCTG	TCTCCAGAGCTCGCTTTACC
RPLP0	CCATCAGCACCACAGCCTTA	GGCGACCTGGAAGTCCAACT
RPLP0 probe	6-FAM-YY-ATCTGCTGCATCTGCTTGGAGCCCA-BHQ1	

2.8 Immunoblotting

A detailed protocol for western blotting was provided in our earlier report (Skov *et al*., 2005). 4-12% Bis-Tris plus precast gels (ThermoFisher) were used for protein electrophoresis. Samples were transferred to nitrocellulose membranes using iBlot dry blotting system (ThermoFisher). The nitrocellulose membranes were blocked for 1 hour with 5% BSA in TBST (TBS with 0.05% Tween 20) and incubated overnight at 4 °C with the respective primary antibodies: Anti-HLA heavy chain (clone EP1395Y, Abcam, 1:4000), anti-β-tubulin (clone TUB2.1, Sigma Aldrich, 1:200), anti-beta2m (1:500), anti-TAP1 (1:500), anti-TAP2 (1:500), anti-LMP2 (1:500) and anti-LMP7 (1:500). TAP1, TAP2, LMP2 and LMP7 specific mAbs have been produced and characterized as described before (Wang *et al*., 2005). The following day, membranes were washed and incubated for 1 hour with the appropriate peroxidase-coupled secondary antibodies (Agilent Technologies, Ratingen, Germany), followed by visualization using the Plus-ECL chemiluminescence detection kit (ThermoFisher).

2.9 MHC-I cell surface expression analysis by flow cytometry

Cell surface expression of HLA class I proteins was determined by flow cytometry as described in our earlier publication (Ritter *et al*., 2017). Briefly, 1×10^6 cells were washed with ice cold PBS. Afterwards, cells were incubated with a FITC-conjugated anti-HLA class I antibody (clone W6/32, BioLegend) in PBS supplemented with 0.1% bovine serum albumin (BSA)for 90 mins at 4°C protected from light. After three washes, cells were stained with 1 µL of 7-AAD for viable/non-viable cell discrimination and analyzed on flow cytometer. Data were analyzed using FlowJo V10.

2.10 Instruction for domatinostat (4SC-202)

Solid domatinostat comes in the form of mesylate salt and has a molecular weight of 619.71 g/mol. For a 50 mM stock solution add 62 µl DMSO into domatinostat powder (one tube); prepare a working stock (10 mM) by dilution in DMSO; prepare solution with desired final concentration in RPMI suppled with P/S (add 10 µl stock solution A to 40 µl RPMI).

2.11 Mycoplasma detection

Material: my-Budget 5 x PCR-Master mix, Artikel-Nr.: 80-62001000;

cells were cultivated 3-4 days before testing; Preheat Thermo Mixer at 95°C.

Primer: Myco-SE 5'-GGG AGC AAA CAG GAT TAG ATA CCC-3'

Myco-AS 5'-TGC ACC ATG TGT CAC TCT GTT AAC CTC-3'

PCR preparation: Total volume per reaction is 10µl:

Component	µl
5x PCR Mastermix	2
Primer 1 myko Se	0.25
Primer 1 myko Sa	0.25
Template	1
H2O	6.5
Total Volume	10

Prepare master mix and store on ice, incubate samples for 10 min at 95°C (spin down shortly, store samples on ice), apply 9 µl master mix per well in a plate or PCR stripe, add 1µl sample. Prepare 2% agarose gel: dissolve 2g agarose powder in 100 ml TAE and microwave for 5 mins, add DNA staining (6µl /100ml) afterwards, pour it directly into the slot and the gel could be

used after 30 minutes. Apply the samples on a 2% agarose gel, run 120V for 45min. Positive samples show a band at 300bp.

2.12 RNA extraction

1. Homogenization and lysis: add 400 μl RNA lysis buffer T to the cell pellet in the tube, incubate the pellet at room temperature for 2 mins, resuspending by pipetting up and down, then incubate for further 3 mins at room temperature.
2. Filtration: place the DNA removing column into a 2.0 ml collection tube and transfer the lysed sample to the DNA removing column, then centrifuge at 10,000 g for approximately 2 mins. After centrifugation discard the DNA removing column.
3. Load and bind: place a perfect binding RNA column into a new 2.0 ml collection tube, add the same volume (400 μl) of isopropanol to the filtrate from step 2 and mix them by pipetting, afterwards, transfer the sample to the perfect bind RNA column, centrifuging the tube at 10,000 g for 2 mins.
4. Washing: add 500 μl RNA washing buffer I to the sample and centrifuge it at 10,000 g for 1 min, afterwards, discard the collection tube with the filtrate and place column into a new 2.0 ml collection tube. Then, add 700 μl completed RNA washing buffer II and centrifuge at 10,000 g for 1 min, afterwards, place it to a new collection tube.
5. Dry: centrifuge the tube at 10,000 g for 3 mins.
6. Elution: Place the RNA column into a new 1.5 ml micro centrifuge tube and add 30 μl sterile RNA free water, incubate the sample at room temperature for 1 min and the centrifuge at 6000 g for 1 min.

2.13 Statistical analysis

Statistical analyses were carried out under the GraphPad Prism 8.0 Software (GraphPad Software Inc., San Diego, CA, USA). For two-group comparisons, significance (two-tailed *P*-value) was carried out with the nonparametric Mann-Whitney test. To compare more than two groups, we used the nonparametric Kruskal-Wallis test along with Dunn's multiple comparison test. *P*-values were assigned as follows and relevant parameters were listed in each figure: **: $P < 0.01$; ***: $P < 0.001$; ****: $P < 0.0001$.

3. Results

3.1 Domatinostat induces a distinct gene expression pattern in MCC cells

The effect of domatinostat treatment on the transcriptome was scrutinized in the classical MCC cell line WaGa. Cells were treated with domatinostat at a concentration of 2.5 µM for 24 hours at 37°C. In line with earlier evidence of epigenetic landscaping and transcriptional regulation by HDAC inhibitors (Halsall *et al*., 2015, Hull *et al*., 2016, Ritter *et al*., 2017), single-cell RNA-sequencing (scRNA-seq) and subsequent cluster assignment revealed a distinct gene signature upon domatinostat treatment (**Figure 1a**). scRNA-seq revealed significant differential expression of 63 genes (adjusted p-value < 0.1) (**Figure 1b**). Functional annotation and pathway enrichment analysis of these differentially expressed genes defined 12 biological processes and/or molecular functions including antigen processing and presentation, apoptosis, transport along microtubule, epithelial cell migration and circadian rhythm (**Figure 1c**). In the following studies, we particularly focused on cell cycle and apoptosis regulation, as well as APM.

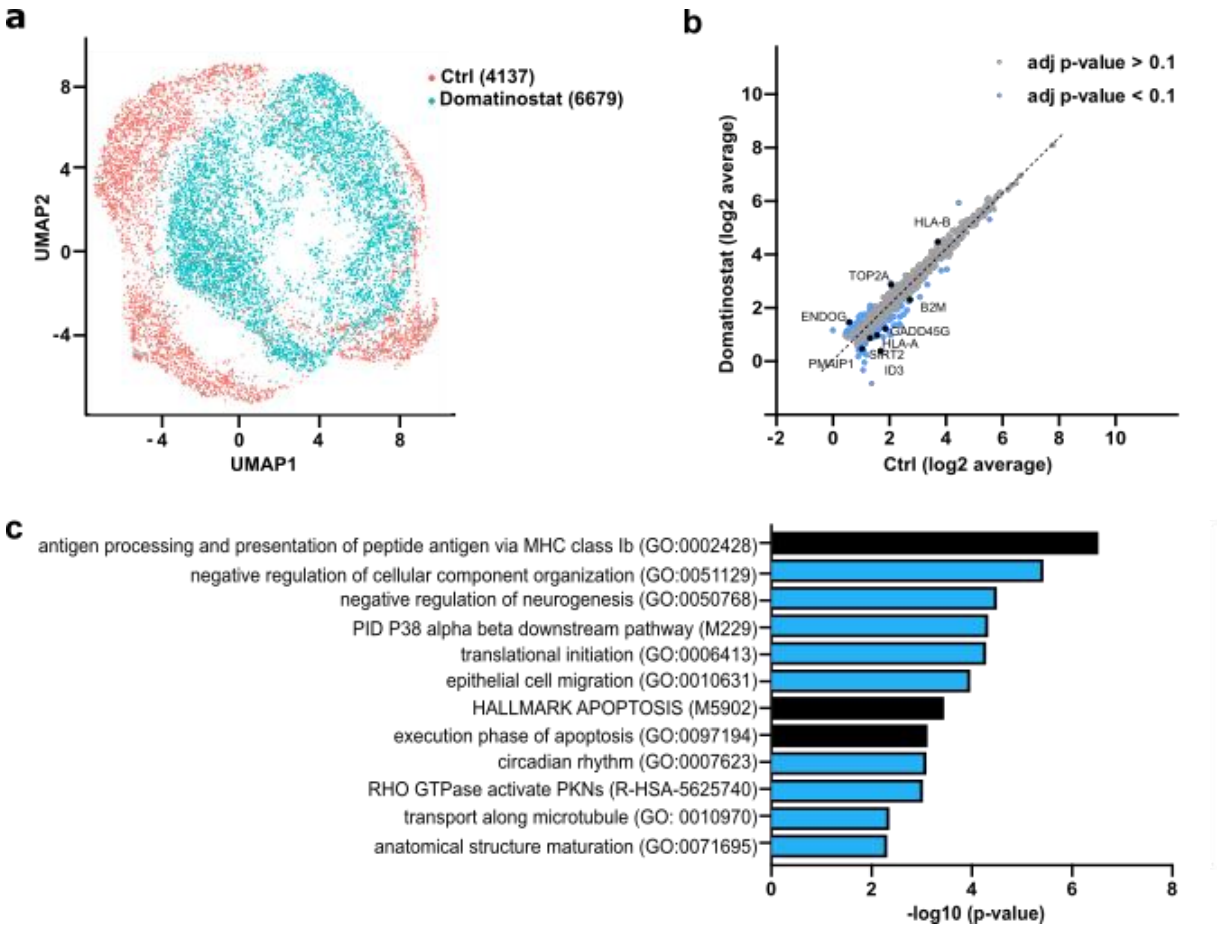

Figure 1: Domatinostat induces global transcriptional changes in MCC cells

WaGa cells were either treated with domatinostat (2.5 µM, 24 hours) or not before being subjected to single-cell RNA-seq. **(a)** Uniform Manifold Approximation and Projection (UMAP) of single-cell gene expression in WaGa cells annotated by treatment. **(b)** Comparison of average single-cell gene expression of domatinostat-treated and control cells. Significantly deregulated genes (adjusted p-value < 0.1) are labeled blue. (**c**) Metascape analysis of significantly enriched pathway terms in differentially expressed genes.

3.2 Induction of G2M cell cycle arrest

Previous reports suggested that HDAC inhibition induces G2M cell cycle arrest in cancer cells (Dong *et al*., 2018). Annotating our scRNA-seq data according to cell cycle phases revealed a more than 1.4-fold increase in number of cells with a gene expression signature for G2M cell cycle phase upon domatinostat treatment (**Figure 2a**). Gene Set Enrichment Analysis (GSEA) demonstrated hallmark of G2M checkpoint gene signature (**Figure 2b**). To functionally test this observation, we performed BrdU incorporation assays for three MCC cell lines WaGa, MKL-1 and MKL-2. These experiments confirmed that G2M cell cycle arrest occurred already after 24 hours of domatinostat treatment. The well-known cell cycle inhibitor nocodazole used as a positive control, also resulted in a G2M arrest after 24 hours of treatment (**Figure 2c**). Quantification of cells in the respective cell cycle phases determined in a series of experiments (n=3), demonstrated a 4-fold increase in the number of cells in G2M phase after domatinostat and a 6-fold increase after nocodazole treatment for 24 hours (**Figure 2d**).

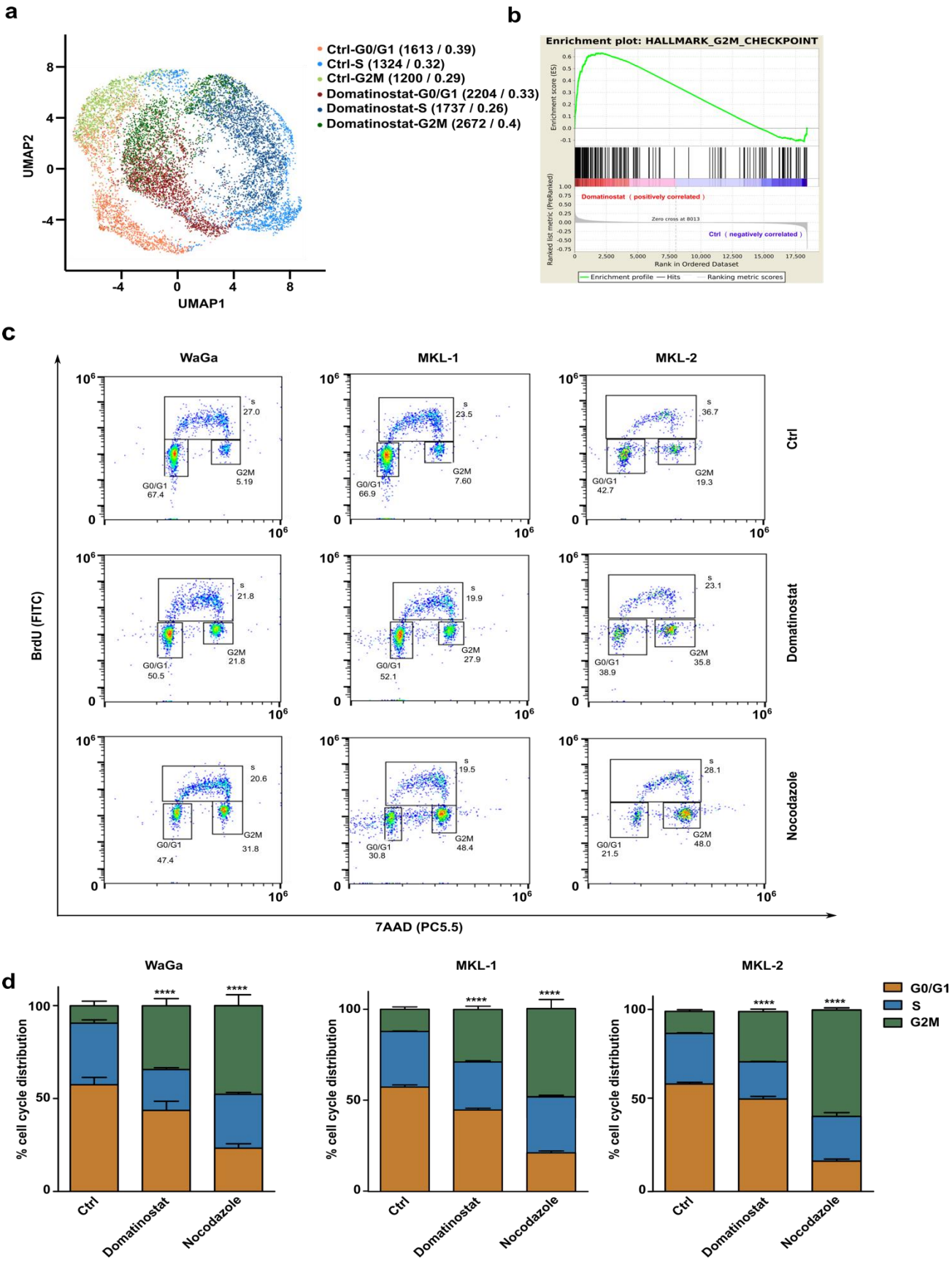

Figure 2: Domatinostat promotes G2M cell cycle arrest

(a) UMAP visualization of single cell gene expression in WaGa cells after domatinostat treatment (2.5 µM, 24 hours) or in controls. Cells were annotated by cell cycle phase and treatment condition. Quantification of cells in the different cell cycle phases were given as absolute numbers and as fractions. (b) Pre-ranked Gene Set Enrichment analysis (GSEA) of the hallmark G2M checkpoint gene set for differentially expressed genes sorted by log2-fold change between domatinostat-treated and control cells (normalized enrichment score (NES)=1,91; false discovery rate (FDR)<0.001). (c) Cell cycle analysis of the indicated MCC cell lines via BrdU incorporation and 7-AAD staining by flow cytometry treated with and without domatinostat (2.5 µM, 24 hours) or nocodazole (100 nM, 24 hours). (d) Quantification of cell cycle profiles in indicated cell lines, represented as mean + / –SD (n=3) and presented as a box plot (P values: ****, P < 0.0001) with individual data points.

3.3 Induction of apoptosis

Persistent G2M arrest of cells has been described as pro-apoptotic (Tyagi *et al*., 2002, Wang *et al*., 2016). In addition, HDAC inhibitors are potent inducers of apoptosis in cancer cells (Bolden *et al*., 2006, Lei *et al*., 2010). Since domatinostat modulated the expression of apoptotic genes in WaGa cells (**Figure 1c**), we next evaluated its impact on cell viability. Indeed, domatinostat treatment reduced the fraction of viable MCC cells (**Figure 3a**). In particular, domatinostat induced apoptosis in WaGa, MKL-1 and MKL-2 cells as detected by an increase in caspase 3/7 activity and the loss of mitochondrial membrane potential ($\Delta\Psi_m$). Notably, MCC cells growing as spheroids dissociated after treatment (**Figure 3b**). Forty-six percent of WaGa, 65.4 % of MKL-1 and 22.13 % of MKL-2 cells underwent apoptosis upon treatment with domatinostat within 24 hours. Again, nocodazole served as positive control; despite the fact that it was more effective to induce G2M arrest, it induced less apoptosis (**Figure 3b-d**). It should be noted that

the fibroblasts, which were not killed by domatinostat **(Figure 3a-d)**, were susceptible to H_2O_2 induced apoptosis (Xiang *et al*., 2016) (**Figure S1**).

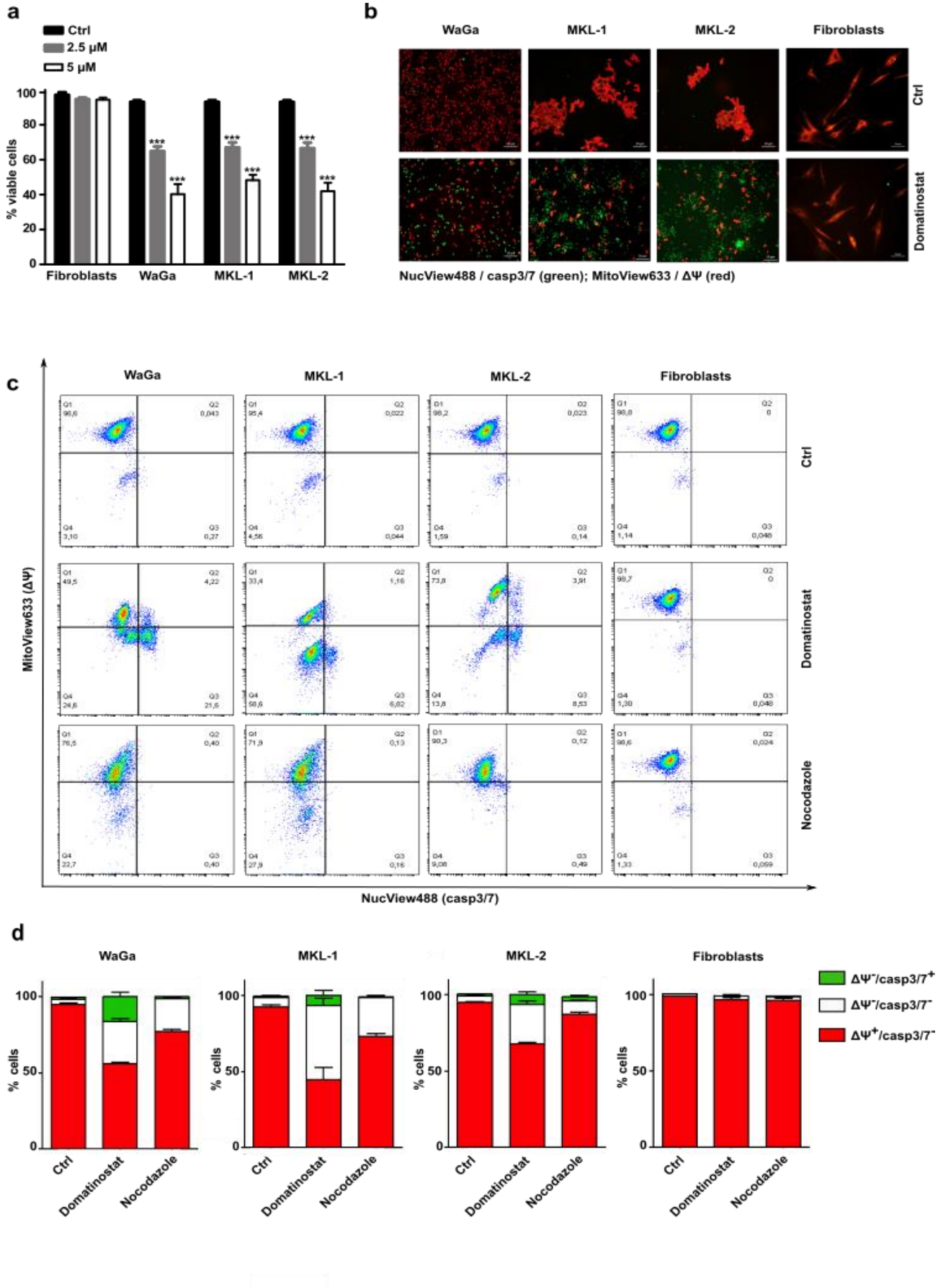

Figure 3: Domatinostat treatment promotes apoptosis in MCC cells

(a) Viability of MCC cell lines WaGa and MKL-1 following a 24 hours treatment with indicated concentrations of domatinostat. **(b-d)** Apoptosis was analyzed with the NucView 488/MitoView 633 Apoptosis Assay Kit. Healthy cells with an intact mitochondrial membrane potential ($\Delta\Psi m^+$) are stained with MitoView 633 (red), while late apoptotic cells (active caspase 3/7) are stained with NucView 488 (green). MCC cell lines and primary fibroblasts were treated with 2.5 µM domatinostat for 24 hours at 37°C. Visualization by fluorescence microscopy **(b)** or flow cytometry **(c)**. Quantification of flow cytometry analysis is given in **(d)** as mean + / – SD (n=3) and presented as a box plot (whiskers: min to max) with individual data points (P values: **, P < 0.01; ***, P < 0.001; ****, P < 0.0001).

3.4 Increased expression of APM genes and MHC class I surface molecules by MCC cells

scRNA-seq analysis demonstrated a domatinostat-induced expression of APM genes in living WaGa cells. We wanted to confirm this observation in additional MCC cell lines. Since domatinostat induced apoptosis in a substantial fraction of, but not all MCC cells, we quantified APM component gene expression in surviving cells, *i.e.*, after enrichment of viable cells. We scrutinized the expression of transporter associated with antigen processing 1 and 2 (TAP1 and TAP2), as well as large multifunctional protease 2 and 7 (LMP2 and LMP7). The induction of these genes and proteins upon treatment with another HDAC inhibitor in MCC was previously reported (Ritter *et al.*, 2017). First, the kinetics of induction of these APM component genes were tested by time course experiments measuring LMP2 and TAP2 mRNA expression in WaGa cells. Four, 8 and 24 hours after treatment with variable domatinostat concentrations were performed. These experiments demonstrated the induction of mRNA expression of these genes after 24 hours in a dose-dependent manner (**Figure 4a**).

The condition demonstrating significant efficacy was used for additional experiments (2.5 µM/24 hours). All of the APM component genes analyzed (LMP2, LMP7, TAP1 and TAP2) were significantly upregulated in the viable cell fraction following treatment with domatinostat (**Figure 4b**). As domatinostat specifically augments APM component gene expression in viable cells, the upregulation of APM component genes is unlikely to be just a consequence of decreased cell viability, as has been described for some forms of immunogenic cell death (Zhou *et al*., 2019). Immunoblots for TAP1, TAP2, LMP2 and LMP7 proteins confirmed the increased expression of all of them upon domatinostat treatment. Furthermore, this induction was paralleled by an increased expression of β2-microglobulin and HLA-A (**Figure 4c, d**).

To test whether HLA class I proteins are expressed in a functional manner and subsequently transported to the plasma membrane, mAb W6/32 targeting HLA class I (Ravindranath *et al*., 2017) was used to detect cell surface expression by flow cytometry in non-permeabilized WaGa and MKL-1 cells. In accordance to the results obtained with whole cell lysates (**Figure 4c, d**), basal expression of HLA class I was low in both cell lines. However, domatinostat induced a concentration-dependent increase of protein expression at the plasma membrane suggesting that functional plasma membrane proteins are transported via the secretory pathway (**Figure 4e, f**).

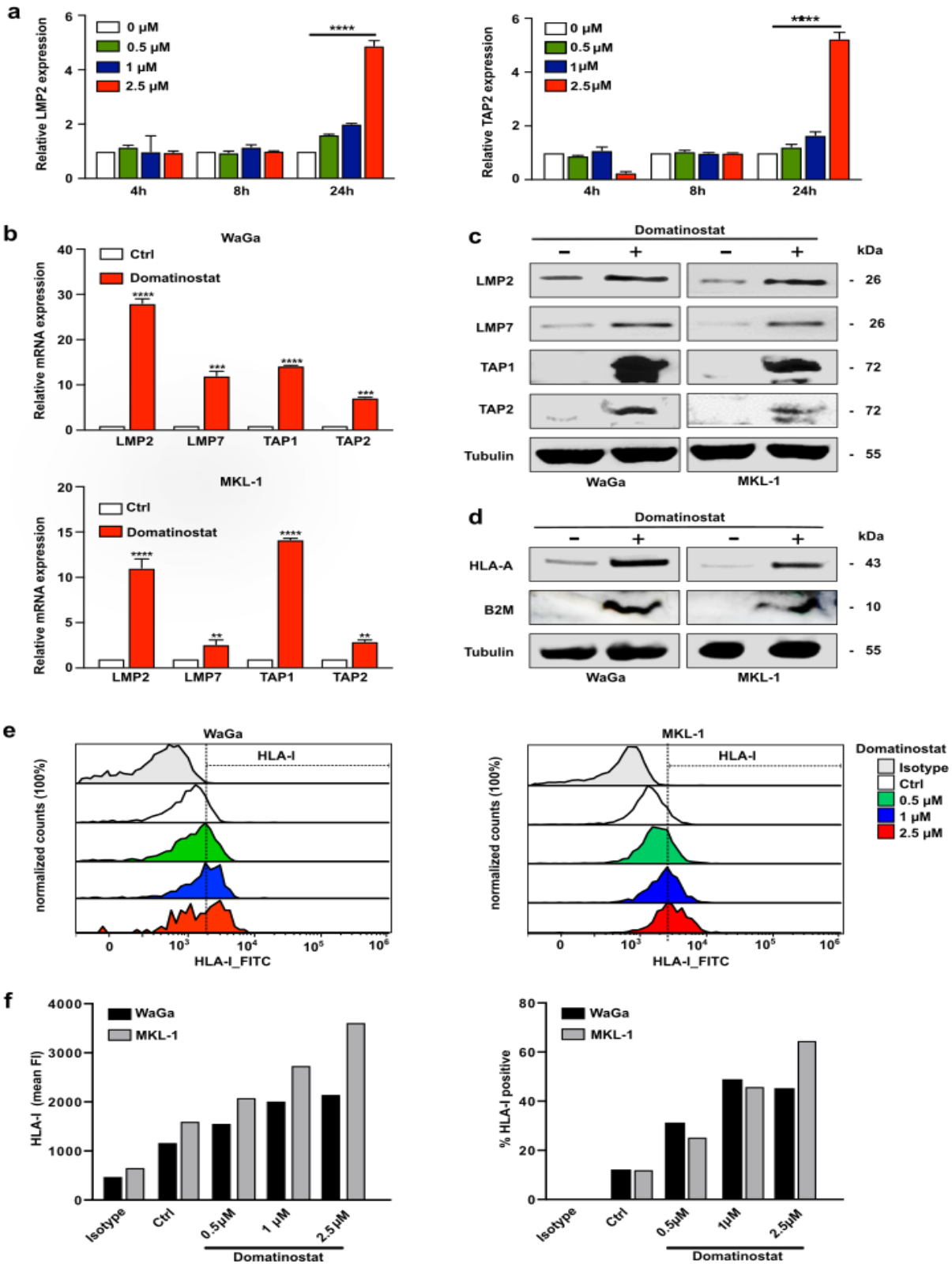

Figure 4: Domatinostat induces expression of APM component gene expression and MHC class I surface expression by MCC cells.

Increased expression of antigen processing machinery genes is mediated by pharmacologic histone deacetylase inhibition. For all experiments the indicated MCC cell lines were analyzed without treatment and after treatment with Domatinostat. **(a)** WaGa cells were treated with the indicated concentrations of domatinostat for 4, 8 and 24 hours at 37 °C. Gene expression of LMP2 and TAP2 was analyzed by RT-PCR in triplicates; CT values were normalized to RPLP0 and calibrated to the ΔCT value of untreated WAGA cells; relative mRNA expression is depicted +SEM for WaGa. The indicated cell lines were analyzed without treatment and after treatment with Domatinostat in different concentration (5 µM, 2.5 µM, 1 µM, 0.5 µM) at different time points (24h, 8h, 4h). **(b)** TAP1, TAP2, LMP2 and LMP7 mRNA expression in WaGa and MKL1 cells treated for 24 hours at 37 °C with 2.5 µM domatinostat was measured by RT-qPCR. Only live cells were included in the experiments. Gene expression relative to control is calculated as mean + / − SD (n=3) and presented as a box plot (**, $P < 0.01$; ***, $P < 0.001$; ****, $P < 0.0001$) with individual data points. **(c)** TAP1, TAP2, LMP2 and LMP7 protein expression in WaGa and MKL-1 cells treated with 2.5 µM domatinostat for 24 hours at 37 °C; β-tubulin was used as a loading control. Viable cells were enriched by Ficoll purification for preparation of whole cell lysates. **(d)** HLA-A and β2-microglobulin (B2M) protein expression in WaGa and MKL-1 cells treated with 2.5 µM domatinostat for 24 hours at 37 °C; β-tubulin was used as a loading control. Viable cells were enriched by Ficoll purification for preparation of whole cell lysates. **(e)** Dose dependent up-regulation of HLA class I (HLA-ABC) cell surface expression. Cells were treated with the indicated concentrations of domatinostat for 24 hours at 37 °C. **(f)** Quantification of HLA-I expression from **(e)** showing % of HLA-I positive cells (right) and mean fluorescence intensity (FI, left).

3.5 Domatinostat treatment does not induce apoptosis in primary skin fibroblasts

As expected, domatinostat treatment induced apoptosis in WaGa, MKL-1, and MKL-2 cells, demonstrated by an increase in caspase 3/7 expression and the loss of mitochondrial membrane potential (ΔΨm). In stark contrast, domatinostat treatment neither induced apoptosis, nor increased cell death in primary skin fibroblast cells, whereas, H_2O_2 treatment, shown to induce apoptosis (Xiang et al., 2016), indeed did. Apoptosis was analyzed with the NucView 488/MitoView 633 Apoptosis Assay Kit. Primary fibroblasts were treated with 2.5 µM domatinostat for 24 hours or H_2O_2 (200 nM) as positive control for apoptosis induction. Healthy cells with an intact mitochondrial membrane potential (ΔΨm+) are stained with MitoView 633 (far red), while apoptotic cells (active caspase 3/7) are stained with NucView 488 (green). Representative fluorescence microscopy images of stained MCC cells and **(Figure 5a)** flow cytometry plots of stained MCC cells **(Figure 5b, c)** were showed here. % cells represented as mean +SD (n=3).

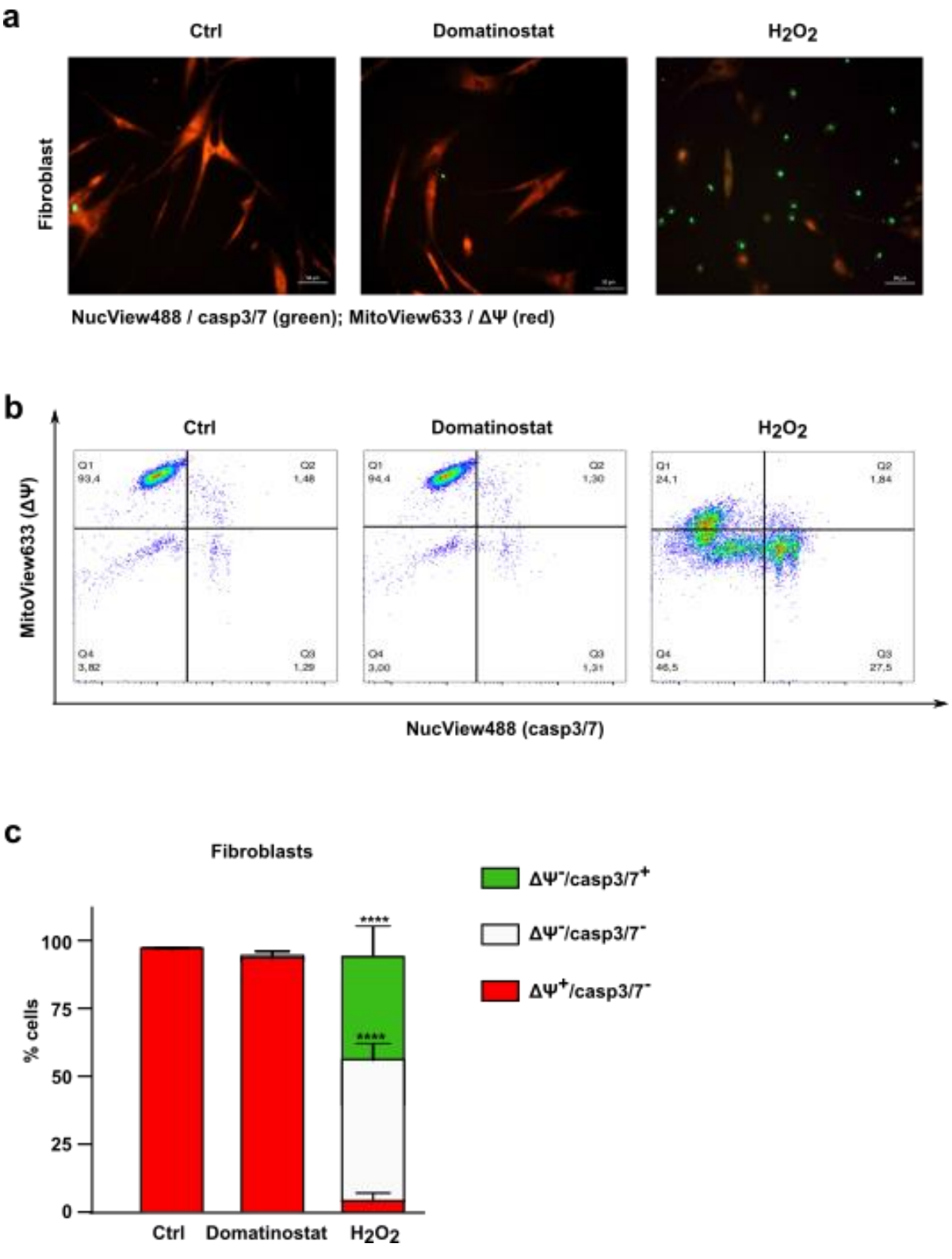

Figure 5: Domatinostat neither induced apoptosis nor increased cell death in primary skin fibroblasts

Apoptosis was analyzed with the NucView 488/MitoView 633 Apoptosis Assay Kit. Healthy cells with an intact mitochondrial membrane potential (ΔΨm+) are stained with MitoView 633 (red), while late apoptotic cells (active caspase 3/7) are stained with NucView 488 (green). Fibroblasts were treated with or without 2.5 μM Domatinostat and with H_2O_2 for 24hrs and then stained with apoptosis dyes for 10 minutes. Representative images for each cell line were captured with a confocal microscope; scale bars represent 100 μM. Red color represents live cells and green ones represent dead cells. Apoptosis assay results analyzed by Flow cytometry. Q1-UL represents healthy cells with high Mito-View and no NucView signal; Q1-LL represents cells losing mitochondrial potential, but still low caspase; Q1-LR represents dead cells with low membrane potential and high caspase. Primary fibroblasts were treated with 2.5 μM domatinostat or H_2O_2 (200 nM) for 24 hours. (a) Representative fluorescence microscopy images or (b) flow cytometry plots. (c) Quantification of flow cytometry analysis is depicted as mean + / − SD (n=3) and presented as stacked bars (P values: ****, $P < 0.0001$).

4. Discussion

Notwithstanding the excellent clinical activity of immune therapy with immune checkpoint inhibitors in MCC, a substantial number of patients do not benefit due to primary or secondary resistance (Kaufman et al., 2018, Nghiem et al., 2019). My lab has previously shown that this may be caused by impaired HLA class I cell surface expression, which impedes recognition of MCC cells by cognate cytotoxic T-cells (Paulson *et al*., 2014, Ritter *et al*., 2017). The impaired HLA class I cell surface expression can be restored by the broad-spectrum HDAC inhibitor vorinostat in combination with the Sp1-inhibitor mithramycin A (Ritter *et al*., 2017). Moreover, broad-spectrum HDAC inhibition by panobinostat enhanced HLA class I surface expression on tumor cells resulting in a brisk infiltration by $CD8^+$ T cells in a patient refractory to immune checkpoint inhibitor therapy (Ugurel *et al*., 2019).

Based on these observations, it appears attractive to combine HDAC inhibitors with immunotherapy (Harms *et al*., 2018). Indeed, it is planned to test the class I HDAC inhibitor domatinostat in combination with the anti-PD-L1 antibody avelumab. Domatinostat is highly specific for HDAC 1-3 with inhibitory constant (Ki) values in the nM range. It is also an inhibitor for the histone demethylase LSD1, which is demonstrated to be a regulator of a wide spectrum of biological processes, involved in cancer development and progression (von Tresckow *et al*., 2019). Concomitant targeting of HDAC and LSD1 proved to be a promising strategy for the cancer treatment as it induces apoptosis by shifting the balance of anti- and pro-apoptotic BCL-2 family proteins (Haydn *et al*., 2017). However, the dual inhibitory activity of domatinostat has not been scrutinized yet and requires additional experiments (von Tresckow *et al*., 2019). By these and other mechanisms, domatinostat has been reported to enhance the infiltration of cytotoxic T cells into tumors of syngeneic mouse models resulting in synergistic effects when combined with immune checkpoint blocking antibodies (Hamm *et al*., 2018).

To provide the requirements for a rational design of translational studies for the MERKLIN trials, we specifically scrutinized the effects of domatinostat on MCC cells *in vitro*.

Domatinostat alone is sufficient to induce HLA class I cell surface expression by boosting APM component gene transcription. In addition, it causes a G2M cell cycle arrest and initiates apoptosis in MCC cells. Interestingly, domatinostat induced G2M phase arrest of MCPyV-positive MCC cell lines already after 24 hours despite the fact that these tumor cell lines have a rather long doubling time (Schrama *et al*., 2019). However, doubling time in cell culture not only reflects the duration of the cell cycle, but also the amount of cell death. Indeed, in MCC tissues, both a high mitotic as well as a high apoptotic rate is observed (Becker J. C. et al., 2017). To functionally address this notion, nocodazole, which induces both G2M arrest and apoptosis, was used as comparator in the cell cycle and apoptosis experiments. Similar to domatinostat, MCC cells were arrested in G2M phase already after 24 hours of treatment. However, less apoptosis was observed in nocodazole treated MCC cells; thus, domatinostat may specifically kill MCPyV-positive MCC cells by induction of apoptosis. Furthermore, scRNA-seq identified transcriptional modulation patterns caused by domatinostat in MCC, among which the apoptosis signature was most prominent. Notably, the observed effects of domatinostat were specific to MCC cells, whereas fibroblasts were unaffected. This is in line with the hypothesis that cancer cells, in contrast to normal cells, are more susceptible to HDAC inhibition as they require low acetylation levels and thus strongly depend on HDAC activity for maintenance of oncogenic phenotype (Cavalli and Heard, 2019).

HDACs are a set of enzymes that can be used to catalyze the deacetylation of proteins, resulting in changes in protein stability or gene expression. HDACs are classified into three categories: class I (HDACs 1-3 and 8), class II (IIa: HDACs 4, 5, 7 and 9; IIb: HDACs 6 and 10) and class IV (HDAC 11) (Haberland *et al*., 2009). Based on the predominance of class I enzymes in cancer cells (Glaser *et al*., 2003), it is assumed that class I-specific HDAC inhibitors may supersede clinical effects of broad-spectrum inhibitors (Karagiannis and El-Osta, 2006). Indeed, the anti-tumoral activity of class I HDAC inhibitors in hematological malignancies and pediatric tumors have been described (von Tresckow *et al*., 2019). In medulloblastoma,

domatinostat treatment inhibits cell viability and downregulates hedgehog signaling significantly. Upregulated proteins such as HDAC2 and HDAC3 are key targets for domatinostat in medulloblastoma (Messerli et al., 2017b). Bretz *et al*. (2019), recently investigated the changes in immune gene expression signatures by RNA-seq of patient samples obtained in the SENSITIZE trial (NCT03278665). This trial evaluates the efficacy of domatinostat combined with pembrolizumab in advanced-stage melanoma patients refractory/non-responding to prior PD-1 blockade. The results from this trial show an increased expression of APM and MHC genes, along with an upregulation of IFN-γ signaling and a pembrolizumab response gene signature (Ayers *et al*., 2017).

In summary, we provide several lines of evidence suggesting that the class I-selective HDAC inhibitor domatinostat may be effective in MCC patients. On one hand, domatinostat induces cell cycle arrest and apoptosis, on the other hand, it boosts antigen presentation in viable cells. In line with this, it has been recently reported that domatinostat increased expression of cancer germline antigens and MHC molecules on cancer cells in vitro and in vivo. Thus, in syngeneic colorectal models, it induces infiltration of cytotoxic T cells into the tumor microenvironment and synergizes with immune checkpoint inhibitors treatment (Bretz A. C. et al., 2019). Taken together, our findings fuel the rationale of a combined therapeutic approach of domatinostat along with checkpoint inhibitors for MCC therapy. Accordingly, clinical trials are already in its initiation phase.

5. Summary

Merkel cell carcinoma (MCC) is a rare, highly aggressive skin cancer for which immune modulation by immune checkpoint inhibitors show remarkable response rates. However, primary or secondary resistance to immunotherapy prevents benefits in a significant proportion of patients. For MCC, one immune escape mechanism is insufficient recognition by T cells due to downregulation of major histocompatibility complex (MHC) class I surface expression.

Histone deacetylase (HDAC) inhibitors have been demonstrated to epigenetically reverse low MHC class I antigen expression caused by downregulation of the antigen processing machinery (APM). Domatinostat, an orally available small molecule inhibitor targeting HDAC class I, is currently in clinical evaluation to overcome resistance to immunotherapy. Here, we present novel preclinical data on its efficacy and mode of action in Merkel cell polyomavirus (MCPyV)-positive MCC. Single-cell RNA-sequencing revealed a distinct gene expression signature of cell cycle arrest upon treatment. Accordingly, functional assays showed that it induced G2M arrest and apoptosis. In surviving cells, APM component gene transcription and translation were up-regulated, consequently increasing MHC class I surface expression. Altogether, domatinostat not only exerts direct anti-tumoral effects, but also restores HLA class I surface expression on MCPyV-positive MCC cells. Therefore, restoring surviving MCC cells' susceptibility to recognition and elimination by cognate cytotoxic T cells.

This work has been accepted for publication in Journal of Investigative Dermatology.

Bibliography

1. Astratenkova, IV., Rogozkin, VA., P. (2019): The Role of Acetylation/Deacetylation of Histones and Transcription Factors in Regulating Metabolism in Skeletal Muscles. J Neurosci. 49(3), 281-8.
2. Ayers, M., Lunceford, J., Nebozhyn, M., Murphy, E., Loboda, A., Kaufman, DR., Albright, A., Cheng, JD., Kang, SP., Shankaran, V., Piha-Paul, SA., Yearley, J., Seiwert, TY., Ribas, A., McClanahan, TK., P. (2017): IFN-gamma-related mRNA profile predicts clinical response to PD-1 blockade. J Clin Invest. 127(8), 2930-40.
3. Barneda-Zahonero, B., Parra, M., P. (2012): Histone deacetylases and cancer. Mol Oncol. 6, 579-89.
4. Barnes, CE., English, DM., Cowley, SM., P. (2019): Acetylation & Co: an expanding repertoire of histone acylations regulates chromatin and transcription. Essays Biochem. 63, 97-107.
5. Becker, JC., Stang, A., DeCaprio, JA., Cerroni, L., Lebbe, C., Veness, M., Nghiem, P., P. (2017): Merkel cell carcinoma. Nat Rev Dis Primers. 3, 17077.
6. Bolden, JE., Peart, MJ., Johnstone, RW., P. (2006): Anticancer activities of histone deacetylase inhibitors. Nat Rev Drug Dis. 5, 769-84.
7. Bretz, AC., Parnitzke, U., Kronthaler, K., Dreker, T., Bartz, R., Hermann, F., Ammendola, A., P. (2019): Wulff, T., Hamm, S., Domatinostat favors the immunotherapy response by modulating the tumor immune microenvironment (TIME). J Immunother Cancer. 7, 294.
8. Cai, L., Michelakos, T., Yamada, T., Fan, S., Wang, X., Schwab, JH., Ferrone, CR., Ferrone, S., P. (2018): Defective HLA class I antigen processing machinery in cancer. Cancer Immunol Immunother. 67, 999-1009.
9. Cavalli, G., Heard, E., P. (2019): Advances in epigenetics link genetics to the environment and disease. Nature. 571, 489-99.

10. Conte, M., De Palma, R., Altucci, L., P. (2018): HDAC inhibitors as epigenetic regulators for cancer immunotherapy. Int J Biochem Cell Biol. 98, 65-74.
11. Dong, Z., Yang, Y., Liu, S., Lu, J., Huang, B., Zhang, Y., P. (2018): HDAC inhibitor PAC-320 induces G2/M cell cycle arrest and apoptosis in human prostate cancer. Oncotarget. 9, 512-23.
12. Dowlatshahi, M., Huang, V., Gehad, AE., Jiang, Y., Calarese, A., Teague, JE., Dorosario, A., Cheng, JW., Nghiem, P., Schanbacher, C., Thakuria, M., Schmults, C., Wang, LC., Clark, RA., P. (2013): Tumor-specific T cells in human Merkel cell carcinomas: a possible role for Tregs and T-cell exhaustion in reducing T-cell responses. J Invest Derma. 133, 1879-89.
13. Eckschlager, T., Plch, J., Stiborova, M., Hrabeta, J., P. (2017): Histone Deacetylase Inhibitors as Anticancer Drugs. Int J Mol Sci. 18.
14. Ediriweera, MK., Tennekoon, KH., Samarakoon, SR., P. (2018): Emerging role of histone deacetylase inhibitors as anti-breast-cancer agents. Drug Discov Today. 24, 685-702.
15. Ellmeier, W., Seiser, C., P. (2018): Histone deacetylase function in CD4(+) T cells. Nat Rev Immunol. 18, 617-34.
16. Fan, S., Wang, Y., Wang, X., Huang, L., Zhang, Y., Liu, X., Zhu, W., P. (2018): Analysis of the affinity of influenza A virus protein epitopes for swine MHC I by a modified in vitro refolding method indicated cross-reactivity between swine and human MHC I specificities. Immunogenetics. 70, 671-80.
17. Fu, M., Wan, F., Li, Z., Zhang, F., P. (2016): 4SC-202 activates ASK1-dependent mitochondrial apoptosis pathway to inhibit hepatocellular carcinoma cells. Biochem Biophys Res Commun. 471, 267-73.

18. Gallinari, P., Di Marco, S., Jones, P., Pallaoro, M., Steinkuhler, C., P. (2007): HDACs, histone deacetylation and gene transcription: from molecular biology to cancer therapeutics. Cell Res. 17, 195-211.
19. Glaser, KB., Li, J., Staver, MJ., Wie, RQ., Albert, DH., Davidsen, SK., P. (2003): Role of class I and class II histone deacetylases in carcinoma cells using siRNA. Biochem Biophys Res Commun. 310, 529-36.
20. Gruber, W., Peer, E., Elmer, DP., Sternberg, C., Tesanovic, S., Del Burgo, P., Coni, S., Canettieri, G., Neureiter, D., Bartz, R., Kohlhof, H., Vitt, D., Aberger, F., P. (2018): Targeting class I histone deacetylases by the novel small molecule inhibitor 4SC-202 blocks oncogenic hedgehog-GLI signaling and overcomes smoothened inhibitor resistance. Int J Cancer. 142, 968-75.
21. Haberland, M., Montgomery, RL., Olson, EN., P. (2009): The many roles of histone deacetylases in development and physiology: implications for disease and therapy. Nature Rev Genet. 10(1), 32-42.
22. Halsall, JA., Turan, N., Wiersma, M., Turner, BM., P. (2015): Cells adapt to the epigenomic disruption caused by histone deacetylase inhibitors through a coordinated, chromatin-mediated transcriptional response. Epigenetics Chromatin. 8, 29.
23. Hamm, S., Wulff, T., Kronthaler, K., Schrepfer, S., Parnitzke, U., Bretz, AC., P. (2018): 4SC-202 increases immunogenicity of tumor cells, induces infiltration of tumor microenvironment with cytotoxic T cells, and primes tumors for combinations with different cancer immunotherapy approaches. Cancer Res, 78.
24. Harms, PW., Harms, KL., Moore, PS., DeCaprio, JA., Nghiem, P., Wong, MKK., Brownell, I., P. (2018): The biology and treatment of Merkel cell carcinoma: current understanding and research priorities. Nat Rev Clin Oncol. 15(12), 763-76.

25. Haydn, T., Metzger, E., Schuele, R., Fulda, S., P. (2017): Concomitant epigenetic targeting of LSD1 and HDAC synergistically induces mitochondrial apoptosis in rhabdomyosarcoma cells. Cell Death Dis. 8(6):e2879-e.
26. He, Y., Tai, S., Deng, M., Fan, Z., Ping, F., He, L., Zhang, C., Huang, Y., Cheng, B., Xia, J., P. (2018): Metformin and 4SC-202 synergistically promote intrinsic cell apoptosis by accelerating DeltaNp63 ubiquitination and degradation in oral squamous cell carcinoma. Cancer Med. 8, 3479-90.
27. Hesbacher, S., Pfitzer, L., Wiedorfer, K., Angermeyer, S., Borst, A., Haferkamp, S., Scholz, CJ., Wobser, M., Schrama, D., Houben, R., P. (2016): RB1 is the crucial target of the Merkel cell polyomavirus Large T antigen in Merkel cell carcinoma cells. Oncotarget. 7(22):32956-68.
28. Houben, R., Shuda, M., Weinkam, R., Schrama, D., Feng, H., Chang, Y., Moore, PS., Becker, JC., P. (2010): Merkel cell polyomavirus-infected Merkel cell carcinoma cells require expression of viral T antigens. J Virol 84, 7064-72.
29. Hull, EE., Montgomery, MR., Leyva, KJ., P. (2016): HDAC Inhibitors as Epigenetic Regulators of the Immune System: Impacts on Cancer Therapy and Inflammatory Diseases. BioMed Res Int. 2016, 8797206.
30. Inui, K., Zhao, Z., Yuan, J., Jayaprakash, S., Le, LTM., Drakulic, S., Sander, B., Golas, MM., P. (2017): Stepwise assembly of functional C-terminal REST/NRSF transcriptional repressor complexes as a drug target. Protein Sci. 26(5), 997-1011.
31. Karagiannis, TC., El-Osta, A., P. (2006): Will broad-spectrum histone deacetylase inhibitors be superseded by more specific compounds? Leukemia, 21, 61.
32. Kaufman, HL., Russell, JS., Hamid, O., Bhatia, S., Terheyden, P., D'Angelo, SP., Shih, KC., Lebbe, C., Milella, M., Brownell, I., Lewis, KD., Lorch, JH., Von Heydebreck, A., Hennessy, M., Nghiem, P., P. (2018): Updated efficacy of avelumab in patients with

previously treated metastatic Merkel cell carcinoma after >/=1 year of follow-up: JAVELIN Merkel 200, a phase 2 clinical trial. J Immunother Cancer. 6, 7.

33. Kowalczyk, E., Filipiak-Strzecka, D., Hamala, P., Smiech, N., Kasprzak, JD., Kusmierek, J., Plachcinska, A., Lipiec, P., P. (2015): Prognostic Implications of Discordant Results of Myocardial Perfusion Single-Photon Emission Computed Tomography and Exercise ECG Test in Patients with Stable Angina. Adv Clin Expe Medicine. 24, 965-71
34. Lei, WW., Zhang, KH., Pan, XC., Wang, DM., Hu, Y., Yang, YN., Song, JG., P. (2010): Histone deacetylase 1 and 2 differentially regulate apoptosis by opposing effects on extracellular signal-regulated kinase 1/2. Cell Death Dis. 1, e44.
35. Li, Y., Seto, E., P. (2016): HDACs and HDAC Inhibitors in Cancer Development and Therapy. Cold Spring Harbor perspectives in medicine. 6.
36. Lipson, EJ., Vincent, JG., Loyo, M., Kagohara, LT., Luber, BS., Wang, H., XU, L., Nayar, SK.,Wang, TS., Sidransky, D., Anders, RA., Topalian, SL., Taube, JM., P. (2013): PD-L1 expression in the Merkel cell carcinoma microenvironment: association with inflammation, Merkel cell polyomavirus and overall survival. Cancer Immunol Res. 1, 54-63.
37. Ma, JE., Brewer, JD., P. (2014): Merkel cell carcinoma in immunosuppressed patients. Cancers. 6(3), 1328-50.
38. Messerli, SM., Hoffman, MM., Gnimpieba, EZ., Kohlhof, H., Bhardwaj, RD., P. (2017): 4SC-202 as a Potential Treatment for the Pediatric Brain Tumor Medulloblastoma. Brain Sci. 7.
39. Miller, RW., Rabkin, CS., P. (1999): Merkel cell carcinoma and melanoma: etiological similarities and differences. Cancer Epidemiol Biomarkers Prev. 8, 153-8.
40. Mishra, VK., Wegwitz, F., Kosinsky, RL., Sen, M., Baumgartner, R., Wulff, T., Siveke, JT., Schildhaus, HU., Najafova, Z., Kari, V., Kohlhof, H., Hessmann, E., Johhsen, SA.,

P. (2017): Histone deacetylase class-I inhibition promotes epithelial gene expression in pancreatic cancer cells in a BRD4- and MYC-dependent manner. Nucleic Acids Res. 45, 6334-49.

41. Moreno-Bost, A., Szmania, S., Stone, K., Garg, T., Hoerring, A., Szymonifka, J., Shaughnessy J, Jr., Barlogie, B., Prentice, HG., Van Rhee, F., P. (2011): Epigenetic modulation of MAGE-A3 antigen expression in multiple myeloma following treatment with the demethylation agent 5-azacitidine and the histone deacetlyase inhibitor MGCD0103. Cytotherapy. 13, 618-28.
42. Nghiem, B., Zhang, X., Lam, HM., True, LD., Coleman, I., Higano, CS., Nelson, PS., Pritchard, CC., Morrissey, C., P. (2016): Mismatch repair enzyme expression in primary and castrate resistant prostate cancer. Asian J Urol. 3(4), 223-8.
43. Nghiem, PT., Bhatia, S., Lipson, EJ., Kudchadkar, RR., Miller, NJ., Annamalai, L., Berry, Sneha., Chartash, EK., Daud, AD., Fling, SP., Friedlander, PA., Kluger, HM., Kohrt, HE., Lundgren, L., Margolin, K., Mitchell, A., Olencki, T., Pardoll, DM., Reddy, SA., Shantha, EM., Sharfman, WH., Sharon, E., Shemanski, LR., Shinahara, MM., Sunshine, JC., Taube, JM., Thompson, JA., Townson, SM., Yearley, JH., Topalian, SL., Cheever, MA., P. (2016): PD-1 Blockade with Pembrolizumab in Advanced Merkel-Cell Carcinoma. N Engl J Med. 374, 2542-52.
44. North, VS., Habib, LA., Yoon, MK., P. (2019): Merkel cell carcinoma of the eyelid: A review. Surv Ophthalmol. 64(5), 659-67.
45. Paulson, KG., Tegeder, A., Willmes, C., Iyer, JG., Afanasiev, OK., Schrama, D., Koba, S., Thibodeau, R., Nagase, K., Simonson, WT., Seo, A., Koelle, DM., Madeleine, M., Bhatia, S., Nahajima, H., Sano, S., Hardwick, JS., Disis, ML., Cleary, MA., Becker, JC., Nghiem, P., P. (2014): Downregulation of MHC-I expression is prevalent but reversible in Merkel cell carcinoma. Cancer Immunol Res. 2, 1071-9.

46. Paulson, KG., Voillet, V., McAfee, MS., Hunter, DS., Wagener, FD., Perdicchio, M., Valente, WJ., Koelle, SJ., Church, N., Thomas, VH., Colunga, AG., Lyer, JG., Kulikauskas, R., Koelle, DM., Pierce, RH., Bielas, J.H., Bhatia, GS., Nghiem, GP., Chapuis, AG., P. (2018): Acquired cancer resistance to combination immunotherapy from transcriptional loss of class I HLA. Nat Commun. 9, 3868.

47. Pinkerneil, M., Hoffmann, MJ., Kohlhof, H., Schulz, WA., Niegisch, G., P. (2016): Evaluation of the Therapeutic Potential of the Novel Isotype Specific HDAC Inhibitor 4SC-202 in Urothelial Carcinoma Cell Lines. Targeted oncology. 11, 783-98.

48. Raffaghello, L., Prigione, I., Bocca, P., Morandi, F., Camoriano, M., Gambini, C., Wang, X., Ferrone, S., Pistoia, V., P. (2005): Multiple defects of the antigen-processing machinery components in human neuroblastoma: immunotherapeutic implications. Oncogene. 24, 4634-44.

49. Ravindranath, MH., Jucaud, V., Ferrone, S., P. (2017): Monitoring native HLA-I trimer specific antibodies in Luminex multiplex single antigen bead assay: Evaluation of beadsets from different manufacturers. J Immunol Methods. 450, 73-80.

50. Ritter, C., Fan, K., Paschen, A., Reker Hardrup, S., Ferrone, S., Nghiem, P., Ugurel, S., Schrama, David., Becker, JC., P. (2017): Epigenetic priming restores the HLA class-I antigen processing machinery expression in Merkel cell carcinoma. Sci Rep. 7, 2290.

51. Ritter, C., Fan K., Paulson, KG., Nghiem, P., Schrama, D., Becker, JC., P. (2016): Reversal of epigenetic silencing of MHC class I chain-related protein A and B improves immune recognition of Merkel cell carcinoma. Sci Rep. 6,21678.

52. Sade-Feldman, M., Jiao, YJ., Chen, JH., Rooney, MS., Barzily-Rokni, M., Eliane, JP., Bjorgaard, SL., Hammond, MR., Vitzthum, H., Blackmon, SM., Frederick, DT., Hazar-Rethinam, M., Nadres, BA., Van Seventer, EE., Shukla, SA., Yizhak, K., Ray, JP., Rosebrock, D., Livitz, D., Adalsteinsson, V., Getz, G., Duncan, LM., Li, B., Corcoran, RB., Lawrence, DP., Stemmer-Rachamimov, A., Boland, GM., Landau, DA., Flaherty,

KT., Sullivan, RJ., Hacohen, N., P. (2017): Resistance to checkpoint blockade therapy through inactivation of antigen presentation. Nat Commun. 8, 1136.

53. Schell, TD., Mylin, LM., Tevethia, SS., Joyce, S., P. (2002): The assembly of functional beta(2)-microglobulin-free MHC class I molecules that interact with peptides and CD8(+) T lymphocytes. Int Immunol. 14, 775-82.
54. Schiller, JT., Lowy, DR., P. (2010): Vaccines to prevent infections by oncoviruses. Annu Rev Microbiol. 64, 23-41.
55. Schrama, D., Sarosi, EM., Adam, C., Ritter, C., Kaemmerer, U., Klopocki, E., Koenig, EM., Utikal, J., Becker, JC., Houben, R., P. (2019): Characterization of six Merkel cell polyomavirus-positive Merkel cell carcinoma cell lines: Integration pattern suggest that large T antigen truncating events occur before or during integration. Int J Cancer. 145(4), 1020-32.
56. Setiadi, AF., Omilusik, K., David, MD., Seipp, RP., Hartikainen, J., Gopaul, R., Choi, KB., Jefferies, WA., P. (2008): Epigenetic enhancement of antigen processing and presentation promotes immune recognition of tumors. Cancer Res. 68, 9601-7.
57. Skov, S., Pedersen, MT., Andresen, L., Straten, PT., Woetmann, A., Odum, N., P. (2005): Cancer cells become susceptible to natural killer cell killing after exposure to histone deacetylase inhibitors due to glycogen synthase kinase-3-dependent expression of MHC class I-related chain A and B. Cancer Res. 65, 11136-45.
58. Stang, A., Becker, JC., Nghiem, P., Ferlay, J., P. (2018): The association between geographic location and incidence of Merkel cell carcinoma in comparison to melanoma: An international assessment. Eur J Cancer. 94, 47-60.
59. Strober, W., P. (2015): Trypan Blue Exclusion Test of Cell Viability. Curr Protoc Immunol. 111, A3.B.1-A3.B.
60. Toker, C., P. (1972): Trabecular carcinoma of the skin. Archives of dermatology. 105, 107-10.

61. Tyagi AK, Singh RP, Agarwal C, Chan DC, Agarwal R. Silibinin strongly synergizes human prostate carcinoma DU145 cells to doxorubicin-induced growth Inhibition, G2-M arrest, and apoptosis. Clin Cancer Res 2002;8(11):3512-9.

62. Ugurel, S., Spassova, I., Wohlfarth, J., Drusio, C., Cherouny, A., Melior, A., Melior, A., Sucker, A., Zimmer, L., Ritter, C., Schadendorf, D., Becker, JC.,. P. (2019): MHC class-I downregulation in PD-1/PD-L1 inhibitor refractory Merkel cell carcinoma and its potential reversal by histone deacetylase inhibition: a case series. Cancer Immunol Immunother. 68, 983-90.

63. Ververis, K., Hiong, A., Karagiannis, TC., Licciardi, PV., P. (2013): Histone deacetylase inhibitors (HDACIs): multitargeted anticancer agents. Biologics. 7, 47-60.

64. von Tresckow, B., Sayehli, C., Aulitzky, WE., Goebeler, ME., Schwab, M., Braz, E., P. (2019): Phase I study of domatinostat (4SC-202), a class I histone deacetylase inhibitor in patients with advanced hematological malignancies. Eur J Haematol. 102, 163-73.

65. Walsh, NM., Fleming, KE., Hanly, JG., Dakin Hache, K., Doucette, S., Ferrara, G., Cerroni, L., P. (2016): A morphological and immunophenotypic map of the immune response in Merkel cell carcinoma. Human pathology. 52, 190-6.

66. Wang, H., Zhang, T., Sun, W., Wang, Z., Zuo, D., Zhou, Z., Li, S., Xu, J., Yin, F., Hua, Y., Cai, Z., P. (2016): Erianin induces G2/M-phase arrest, apoptosis, and autophagy via the ROS/JNK signaling pathway in human osteosarcoma cells in vitro and in vivo. Cell Death Dis. 7, e2247.

67. Wang, X., Campoli, M., Cho, HS., Ogino, T., Bandoh, N., Shen, J., Hur, SY., Kageshita, T., Ferrone, S., P. (2005): A method to generate antigen-specific mAb capable of staining formalin-fixed, paraffin-embedded tissue sections. J Immunol Methods. 299, 139-51.

68. West, AC., Smyth, MJ., Johnstone, RW., P. (2014): The anticancer effects of HDAC inhibitors require the immune system. Oncoimmunology. 3(1).

69. Wobser, M., Weber, A., Glunz, A., Tauch, S., Seitz, K., Butelmann, T., Hesbacher, S., Goebeler, M., Bartz, R., Kohlhof, H., Schrama, D., Houben, R., P. (2019): Elucidating the mechanism of action of domatinostat (4SC-202) in cutaneous T cell lymphoma cells. J Hematol Oncol. 12, 30.

70. Xiang, J., Wan, C., Guo, R., Guo, D., P. (2016): Is Hydrogen Peroxide a Suitable Apoptosis Inducer for All Cell Types? BioMed Res Int. 2016, 7343965.

71. Zheng, GXY., Terry, JM., Belgrader, P., Ryvkin, P., Bent, ZW., Wilson, R., Ziraldo, SB., Wheeler, TD., McDermott, GP., Zhu, J., Gregory, MT., Shuga, J., Underwood, DA., Nishimura, SY., Schnall-Levin, M., Wyatt, PW., Hindson, CM., Bharadwaj, R., Wong, A., Ness, KD., Beppu, LW., Deeg, H., McFarland, C., Loeb, KR., Valente, WJ., Ericson, NG., Stevens, EA., Radich, J., Mikkelsen, TS., Hindson, BJ., Bielas, JH., P. (2017): Massively parallel digital transcriptional profiling of single cells. Nat Commun. 8, 14049-.

72. Zheng, H., Zhao, W., Yan, C., Watson, CC., Massengill, M., Xie, M., Massengill, C., Noyes, DR., Martinez, GV., Afzal, R., Chen, Z., Ren, X., Antonis, SJ., Haura, EB., Ruffell, B., Beg, AA., P. (2016): HDAC Inhibitors Enhance T-Cell Chemokine Expression and Augment Response to PD-1 Immunotherapy in Lung Adenocarcinoma. Clin Cancer Res. 22, 4119-32.

73. Zhijun, H., Shusheng, W., Han, M., Jianping, L., Li-Sen, Q., Dechun, L., P. (2016): Pre-clinical characterization of 4SC-202, a novel class I HDAC inhibitor, against colorectal cancer cells. Tumour biology. 37, 10257-67.

74. Zhou, J., Wang, G., Chen, Y., Wang, H., Hua, Y., Cai, Z., P. (2019): Immunogenic cell death in cancer therapy: Present and emerging inducers. J Cell Mol Med. 23, 4854-65.

List of tables and figures

List of abbreviation

APM	antigen processing and presentation machinery
CPI	immune checkpoint inhibitors
HDAC	histone deacetylase
HLA	human leukocyte antigen
LMP.	large multifunctional protease
MCC	Merkel cell carcinoma
MHC	major histocompatibility complex
ScRNA-seq	single-cell RNA sequencing
TAP	transporter associated with antigen processing
Ab	Antibody
DNA	Deoxyribonucleic acid
MCPyV	Merkel cell polyomavirus
mRNA	messenger ribonucleic acid
PCR	polymerase chain reaction
WB	Western blot/blotting

Acknowledgement

Upon the completion of my MD thesis, I would like to express my grateful to all the people who gave me support as well as encouragement during this period. First of all, I would like to express my deep gratitude to China Scholarship Council (CSC), thanks for all the support from them. Besides, I am really grateful for the chance to spend these years working in an enthusiastic lab. Secondly, my special acknowledgment would definitely to my respectful supervisor, Professor Jürgen Becker who have offered me encouragement and have taught me a lot associated with science. During the period, he has given me valuable advices in my project design and studies. In the preparation of my first paper manuscript, he took a lot of effort reading through and modifying each draft, providing me with inspiring suggestions. What is more, I am really grateful to my colleagues in our lab whom I get tremendous courage as well as science skills and technologies. I have benefited from many of my colleagues. Jan Gravemeyer and Kai Horny, they taught me a lot associated with bio-informatics. Shakhlo Muminova, Ivelina Spassova, Lukas Peiffer, Ashwin Sriram, Lei Zhang and Kaiji Fan, they helped me a lot on experimental stuff. Here I also want to express my deep thanks to Viola De Temple for reading through the thesis for me. Also, I would like to express my gratitude to Corinna Wülbeck, Angela Hebel-Cherouny and Johanna Schwinn for all the help from them. I am really gratitude it and will regard it as treasure in my life in spending three years working in an enthusiastic lab. At the meantime, I also would like to express my deep thanks to Anne Catherine Bretz who helped me a lot considering this domatinostat project, both for the data analyze and paper manuscript modification. Finally, the most gratitude from my heart to my families who have offered me great support and help. Thanks for all the loving considerations for me during these years and help without any words of complaint. Furthermore, I want to express appreciation for the help from University Hospital Essen.

Curriculum Vitae

The curriculum vitae is not included in the online version for data protection reasons.